Mon. Not. R. Astron. Soc. **354,** 753–762 (2004) doi:10.1111/j.1365-2966.2004.08236.x

Nuclear stellar discs in low-luminosity elliptical galaxies: NGC 4458 and 4478

L. Morelli,[1,2]★ C. Halliday,[3] E. M. Corsini,[1] A. Pizzella,[1] D. Thomas,[4] R. P. Saglia,[4] R. L. Davies,[5] R. Bender,[4,6] M. Birkinshaw[7] and F. Bertola[1]

[1]*Dipartimento di Astronomia, Università di Padova, vicolo dell'Osservatorio 2, I-35122 Padova, Italy*
[2]*European Southern Observatory, 3107 Alonso de Cordova, Santiago, Chile*
[3]*INAF-Osservatorio Astronomico di Padova, vicolo dell'Osservatorio 5, I-35122 Padova, Italy*
[4]*Max-Planck Institut für extraterrestrische Physik, Giessenbachstrasse, D-85748 Garching, Germany*
[5]*Department of Astrophysics, University of Oxford, Keble Road, Oxford OX1 3RH*
[6]*Universitäs-Sternwarte, Scheinerstrasse 1, D-81679 Muenchen, Germany*
[7]*H. H. Wills Physics Laboratory, University of Bristol, Tyndall Avenue, Bristol BS8 1TL*

Accepted 2004 July 19. Received 2004 July 12; in original form 2004 May 12

ABSTRACT

We present the detection of nuclear stellar discs in the low-luminosity elliptical galaxies, NGC 4458 and 4478, which are known to host a kinematically decoupled core. Using archival *Hubble Space Telescope* imaging, and available absorption line-strength index data based on ground-based spectroscopy, we investigate the photometric parameters and the properties of the stellar populations of these central structures. Their scalelength, h, and face-on central surface brightness, μ_0^c, fit on the μ_0^c –h relation for galaxy discs. For NGC 4458, these parameters are typical for nuclear discs, while the same quantities for NGC 4478 lie between those of nuclear discs and the discs of discy ellipticals. We present Lick/Image Dissector Scanner (IDS) absorption line-strength measurements of Hβ, Mg b and $\langle$Fe$\rangle$ along the major and minor axes of the galaxies. We model these data with simple stellar populations that account for the α/Fe overabundance. The counter-rotating central disc of NGC 4458 is found to have similar properties to the decoupled cores of bright ellipticals. This galaxy has been found to be uniformly old despite being counter-rotating. In contrast, the cold central disc of NGC 4478 is younger, richer in metals and less overabundant than the main body of the galaxy. This points to a prolonged star formation history, typical of an undisturbed disc-like, gas-rich (possibly pre-enriched) structure.

Key words: galaxies: abundances – galaxies: elliptical and lenticular, cD – galaxies: evolution – galaxies: formation – galaxies: kinematics and dynamics – galaxies: photometry.

1 INTRODUCTION

In recent years, the subarcsec resolution of the *Hubble Space Telescope* (*HST*) has allowed the study of galactic nuclei, unveiling the presence of distinct components such as small-scale stellar discs (see Pizzella et al. 2002 and references therein) and nuclear clusters (Carollo et al. 1997; Böker et al. 2002; Graham & Guzmán 2003). To date surface-brightness distributions of nuclear stellar discs (NSDs) have been measured for only a few S0s (Kormendy et al. 1996; Scorza & van den Bosch 1998; van den Bosch, Jaffe & van der Marel 1998) and early-type spiral galaxies (Pizzella et al. 2002). They have smaller scalelengths (∼10–30 pc) and higher central surface brightnesses (∼15–19 mag arcsec^{-2} in the V band) with respect to those of embedded stellar discs, which have been found in several elliptical and lenticular galaxies (e.g. Scorza & Bender 1995, hereafter SB95). Although only a few NSDs have been studied in detail, they may be quite a common structure in the central regions of spheroids. Indeed, nuclear discs of gas, dust and stars have been clearly detected in a large number of early-type galaxies (e.g. Jaffe et al. 1994; Lauer et al. 1995; van Dokkum & Franx 1995; Carollo et al. 1997; Faber et al. 1997; Tomita et al. 2000; Kormendy & Gebhardt 2001; Tran et al. 2001; Trujillo et al. 2004), but the photometric parameters of such discs have not yet been derived. Furthermore, *HST* imaging in near-infrared bandpasses has provided indirect signatures of the presence of NSDs as discy isophotes in the nuclei of early-type galaxies (Ravindranath et al. 2001) or photometrically distinct exponential components in bulges (Balcells et al. 2003; Balcells, Graham & Peletier 2004). The existence of NSDs suggests that the continuity of the disc properties, with a smooth

★E-mail: morelli@pd.astro.it

variation of scale parameters from spirals to discy ellipticals along a sequence of decreasing disc-to-bulge ratio (Kormendy & Bender 1996), could be extended to nuclear scales (van den Bosch 1998). In this framework, NSDs could provide important clues to the assembly scenario of their host galaxies.

In the current picture, the NSDs observed in bulges of S0s and spiral galaxies are believed to have formed either from a secular evolution of a nuclear bar (e.g. NGC 4570; Scorza & van den Bosch 1998; van den Bosch & Emsellem 1998; van den Bosch et al. 1998) or as the end result of a merging event (e.g. NGC 4698; Bertola et al. 1999; Pizzella et al. 2002). Each of these scenarios is likely to be correct for some but not for all the objects. In both scenarios, the gas is efficiently directed toward the galaxy centre, where it first dissipates and settles on to an equilibrium plane and then forms into stars. Although the decoupled kinematics strongly suggest a later infall (e.g. NGC 4486A; Kormendy & Gebhardt 2001) or merger (e.g. Holley-Bockelmann & Richstone 2000), the frequently indistinguishable star formation history remains an enigma. Yet, these processes are expected to lead to distinct features in stellar populations of NSDs and surrounding spheroids. The measurement of the kinematics of some early-type galaxies (elliptical and S0 galaxies) has revealed evidence for kinematically decoupled or peculiar galaxy cores (see Bertola & Corsini 1999, for a review), strongly indicative of formation by galaxy–galaxy merging (e.g. Kormendy 1984; see Mehlert et al. 1998 and references therein). Such kinematically distinct cores have been associated with a central disc component (e.g. Rix & White 1992; Mehlert et al. 1998). However, triaxial galaxies with radius-dependent ellipsoids can, in projection, mimic kinematically decoupled cores (see Arnold, de & Hunter 1994, and references therein). Spectroscopic absorption line-strength indices (Faber et al. 1985; Trager et al. 1998) constrain the luminosity-weighted stellar population age, metallicity and alpha-element overabundance by comparison with evolutionary population synthesis models (Worthey 1994; Maraston 1998; Tantalo, Chiosi & Bressan 1998; Vazdekis 1999; Bruzual & Charlot 2003; Thomas, Maraston & Bender 2003, hereafter TMB). Absorption line-strength indices have been measured out to one effective radii for elliptical galaxies (e.g. Davies, Sadler & Peletier 1993; González 1993; Halliday 1999; Mehlert et al. 2000). Such measurements can distinguish between merging and dissipational formation scenarios by the constraint of metallicity gradients, dating of the latest episode of star formation and the measurement of the time-scale over which the bulk of the star formation has taken place. In Davies et al. (1993), Mehlert et al. (2003) and the analysis of literature data by Kobayashi & Arimoto (1999), it has been found that elliptical galaxies have gradients in metallicity shallower than predicted by dissipational collapse models. Mehlert et al. (1998) presented spectroscopic line-strength data and *HST* archive imaging for two Coma cluster galaxies with kinematically decoupled cores and found little evidence that the cores have experienced different star formation histories from their parent galaxies. Using wide-field spectroscopic maps of NGC 4365 acquired using the SAURON instrument, Davies et al. (2001) presented evidence for a metal-rich core but constant age and α/Fe enhancement for both the kinematically distinct core and parent galaxy. Both studies are consistent with the core and the main galaxy having experienced similar star formation histories.

In this paper, we use archival *HST* imaging and ground-based spectroscopy to investigate the photometric parameters and stellar population diagnostics of the NSDs hosted by the two Virgo galaxies, NGC 4458 and 4478. NGC 4458 and 4478 are classified as E0-1 (de Vaucouleurs et al. 1991, hereafter RC3) and E2 (Sandage & Tammann 1981; RC3), respectively. They are both low-luminosity ellipticals with $M_B^0 \sim -18$ (RC3) at a distance of 12.6 Mpc (Tully 1988; $H_0 = 100$ km s^{-1} Mpc^{-1}). They have a power-law central luminosity profile (Ferrarese et al. 1994; Faber et al. 1997; Rest et al. 2001) and both galaxies show deviations from the $r^{1/4}$ law in their outskirts (Michard 1985; Prugniel, Nieto & Simien 1987; Caon, Capaccioli & Rampazzo 1990; Peletier et al. 1990), which have been explained as a result of tidal interaction with NGC 4461 and 4486. Recently, the stellar kinematics along the major and minor axes of NGC 4458 and 4478 have been measured by Halliday et al. (2001), who found the signature of a kinematically decoupled core in their inner $\sim$5 arcsec. In particular, NGC 4458 has a clear counter-rotating core along the major axis, while NGC 4478 has a cold component detected along both the major and the minor axes.

In Section 2 we perform the photometric analysis of the archival *HST* images of the nuclei of NGC 4458 and 4478 in order to derive the surface-brightness profiles and scale parameters of their NSDs. In Section 3 we present the absorption line-strength indices as a function of radius of the major and minor axes of both galaxies from the thesis research of Halliday (1999). In Section 4 we combine photometric and spectroscopic results to assess age, metallicity and overabundances of stellar populations of the two NSDs and surrounding spheroids. This has allowed us to suggest possible formation and evolution scenarios for NGC 4458 and 4478. We summarize our conclusions in Section 5.

2 PHOTOMETRIC PARAMETERS

2.1 Data reduction

We retrieved Wide-Field Planetary Camera 2 (WFPC2) images of NGC 4458 and 4478 from the *HST* archive. Data for the filter F814W were selected as a compromise between obtaining data in identical bandpasses for both galaxies and minimizing the effects of dust on photometric measurements. Total exposure times were 1120 s for NGC 4458 (five exposures, Prog. Id. 5512, P.I. S. M. Faber) and 1600 s for NGC 4478 (two exposures, Prog. Id. 6587, P.I. D. Richstone). All exposures were taken with the telescope guiding in fine lock, which typically gave an rms tracking error of 0.003 arcsec. We focused our attention on the Planetary Camera (PC) chip where the nucleus of both galaxies was centred. This consists of 800×800 pixels of 0.0455×0.0455 arcsec^2 each, yielding a field of view of about 36×36 arcsec^2. The images were calibrated using the standard reduction pipeline maintained by the Space Telescope Science Institute (STScI). Reduction steps include bias subtraction, dark current subtraction and flat-fielding, and are described in detail in Holtzman et al. (1995a). Subsequent reduction was completed using standard tasks in the STSDAS package of IRAF.[1] Bad pixels were corrected by means of a linear one-dimensional interpolation using the data quality files and the WFIXUP task. Different images of the same target were aligned and combined using IMSHIFT and knowledge of the offset shifts. Cosmic ray events were removed using the task CRREJ. The cosmic-ray removal and bad pixel correction were checked by inspection of the residual images between the cleaned and combined image and each of the original frames. Residual cosmic rays and bad pixels in the PC were corrected by manually editing the combined image with IMEDIT. The sky level ($\sim$1 count pixel^{-1})

[1] IRAF is distributed by the National Optical Astronomy Observatories (NOAO), which is operated by the Association of Universities for Research in Astronomy (AURA) Inc., under contract with the National Science Foundation.

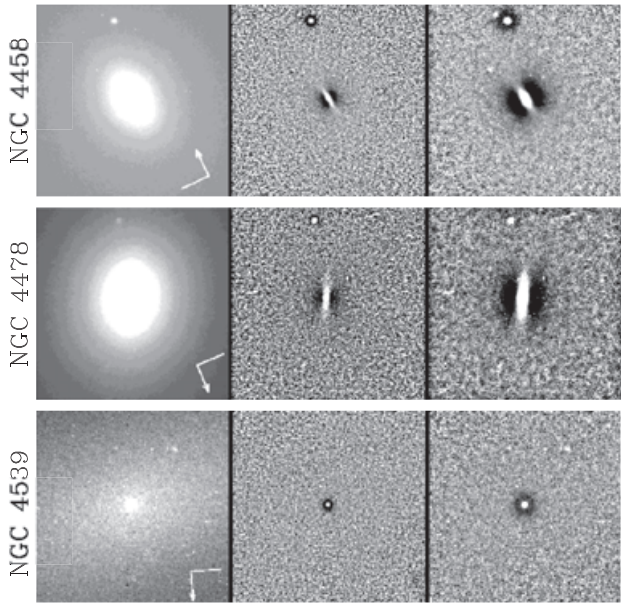

Figure 1. Left panels: WFPC2/F814W images of NGC 4458 and 4478 (for which nuclear discs were detected) and NGC 4539 (for which a nuclear disc was not detected). The size of the plotted region is 19.3 × 19.3 arcsec^2. The orientation is specified by the arrow indicating north and the segment indicating east in the lower-right corner of each panel. Middle and right panels: unsharp masking of the WFPC2/F814W images obtained with $\sigma =$ 2 and 6 pixels, respectively. Sizes and orientations are as in the left-hand panels.

was determined from regions free of sources in the Wide-Field chips and subtracted from the PC frame after appropriate scaling.

2.2 Detection of nuclear discs

To test for the presence of a NSD in NGC 4458 and 4478, we constructed the unsharp-masked image of the PC frame using an identical procedure to that of Pizzella et al. (2002). We divided each image by itself after convolution by a circular Gaussian of width $\sigma =$ 2 and 6 pixels, corresponding to 0.09 and 0.27 arcsec, respectively (Fig. 1). This procedure enhanced any surface-brightness fluctuation and non-circular structure extending over a spatial region comparable to the σ of the smoothing Gaussian. Two values of σ were adopted to attempt the identification of structures with different scalelengths.

A highly elongated structure is clearly visible in the nucleus of each galaxy. These structures are not artefacts of the unsharp-masking procedure. In Fig. 1 we show as a counter-example the unsharp-masked image of NGC 4539, which has been obtained using an identical method to that for NGC 4458 and 4478; we clearly do not detect an elongated disc-like structure. Moreover the nuclear structures of NGC 4458 and 4478 are associated with a central increase in ellipticity measured by performing an isophotal analysis using the IRAF task ELLIPSE (Fig. 2).

We analysed the isophotal profiles of both galaxies by first masking foreground stars and then fitting ellipses to the isophotes. We allowed the centres of the ellipses to vary, to test whether the galaxies were disturbed. Within the errors of the fits, we found no evidence of variations in the fitted centre. The ellipse fitting was repeated with the ellipse centres fixed. The resulting azimuthally averaged surface brightness, ellipticity, position angle, the fourth (a_4) and sixth (a_6) cosine Fourier coefficients profiles are presented in Fig. 2. In

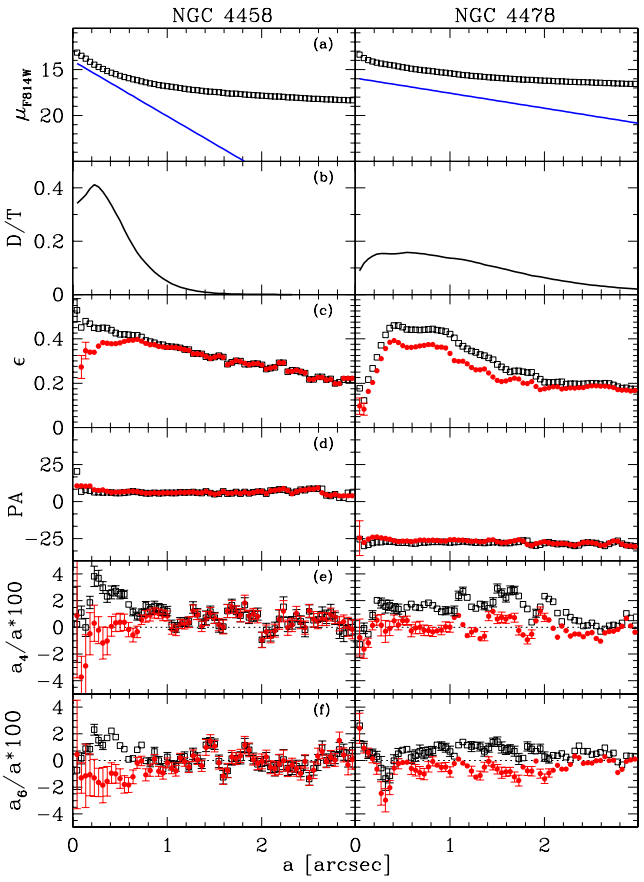

Figure 2. (a) Radial profiles of surface brightness of NGC 4458 (left panel) and NGC 4478 (right panel) after deconvolution (open squares) are compared to those of their nuclear discs (thick lines). (b) Radial profiles of the fraction of total luminosity contributed by the nuclear disc of NGC 4458 (left panel) and NGC 4478 (right panel). Radial profiles of (c) ellipticity, (d) position angle, (e) a_4 and (f) a_6 Fourier coefficients before (open squares) and after (filled circles) the subtraction of the best-fitting model for the nuclear disc of NGC 4458 (left panels) and NGC 4478 (right panels).

the innermost ∼2 arcsec we measured positive values of the a_4 and a_6 Fourier coefficients, which describe the discy deviation of the isophotes from pure ellipses (Jedrzejewski 1987). These photometric features have been also observed in the *HST*/F555W image for NGC 4458 (Lauer et al. 1995; Trujillo et al. 2004) and in the *HST*/F702W image of NGC 4478 (van den Bosch et al. 1994; Rest et al. 2001; Trujillo et al. 2004) and confirm the presence of a NSD in both galaxies.

2.3 Photometric decomposition

2.3.1 Photometric parameters of the nuclear discs with the Scorza & Bender method

After establishing the existence of NSDs, we measured their photometric properties using the method described by SB95. This method is based on the assumption that isophotal disciness is the result of the superimposition of a spheroidal component (which is either a host elliptical galaxy or a bulge component) and an inclined disc. The two components are assumed to have both perfectly elliptical isophotes with constant but different ellipticities. When adopting this technique to study the innermost regions of galaxies, it is essential to

restore the images from the effects of the *HST* point spread function (PSF) in order to properly derive the photometric parameters of the NSDs, as shown by Scorza & van den Bosch (1998). Such deconvolution was performed through the Richardson–Lucy method by means of the IRAF task LUCY. Although susceptible to noise amplification, this algorithm was shown by van den Bosch et al. (1998) to lead to a restored surface-brightness distribution comparable to that obtained using a multiGaussian representation (Monnet, Bacon & Emsellem 1992; Cappellari 2002). We believe that the results obtained by van den Bosch et al. (1998) are directly applicable to our case: we are dealing with images obtained with similar or longer integration times, galaxies with less steep surface-brightness profiles and NSDs with equal or larger scalelengths. We decided to deconvolve images with the number of iterations between three and six. A larger number of iterations does not affect the result of the decomposition but does amplify the noise. For each given image and nucleus position on the PC, we adopted a model PSF calculated using the TINY-TIM package (Krist & Hook 1999). No correction for telescope jitter was necessary. The SB95 method consists of the iterative subtraction of a thin disc model characterized by an exponential surface-brightness profile with central surface brightness I_0 and radial scalelength h, and by an axial ratio b/a. The disc parameters are adjusted until the departures from perfect ellipses are minimized (i.e. a_4 and a_6 are close to zero). For each disc model, we obtained the disc-free image of the galaxy by subtracting the disc model from the galaxy image. We performed an isophotal analysis on the disc-free image using the IRAF task ELLIPSE. We defined

$$\chi^2 = \sum_{i=1}^{N} \frac{a^2_{4,\mathrm{disc\text{-}free}}(i)}{\sigma(i)^2}, \qquad (1)$$

where $a_{4,\mathrm{disc\text{-}free}}(i) \pm \sigma(i)$ is the value of the a_4 Fourier coefficient measured for the ith isophote in the disc-free image, and N is the number of fitted isophotes. We assumed $\sigma(i) = 0.01$ as a typical error on $a_{4,\mathrm{disc\text{-}free}}$ for all the isophotes in the region of the NSD. We defined the reduced χ^2 as $\chi^2_\nu = \chi^2/(N - M)$, where $M = 3$ is the number of free parameters, namely I_0, h and b/a. According to our technique for photometric decomposition the minimum value of $\chi^2_\nu \equiv \chi^2_{\nu,\mathrm{min}}$ corresponds to the best-fitting model of the NSD. We found $\chi^2_{\nu,\mathrm{min}} = 0.43$ for NGC 4458 and $\chi^2_{\nu,\mathrm{min}} = 0.34$ for NGC 4478. We determined $\Delta\chi^2_\nu \equiv \chi^2_\nu - \chi^2_{\nu,\mathrm{min}}$ and derived its confidence levels under the assumption that the errors are normally distributed (Press et al. 1992). The resulting contour plots of χ^2_ν are shown in Fig. 3 and they allowed us to derive the best-fitting values of I_0, h and b/a and their 1σ errors.

We derived the Johnson V-band central surface brightness of the NSDs from the *HST* VEGAMAG system (Holtzman et al. 1995b) using the STSDAS task SYNPHOT. Because this correction depends on the galaxy spectral energy distribution, it has been calculated using the spectral template for elliptical galaxies by Kinney et al. (1996). The resulting relation is $V - m_{\mathrm{F814W}} = 1.33$. We derived the scalelength of the NSDs assuming a distance of 12.6 Mpc for both galaxies. The inclination of NSDs has been calculated as

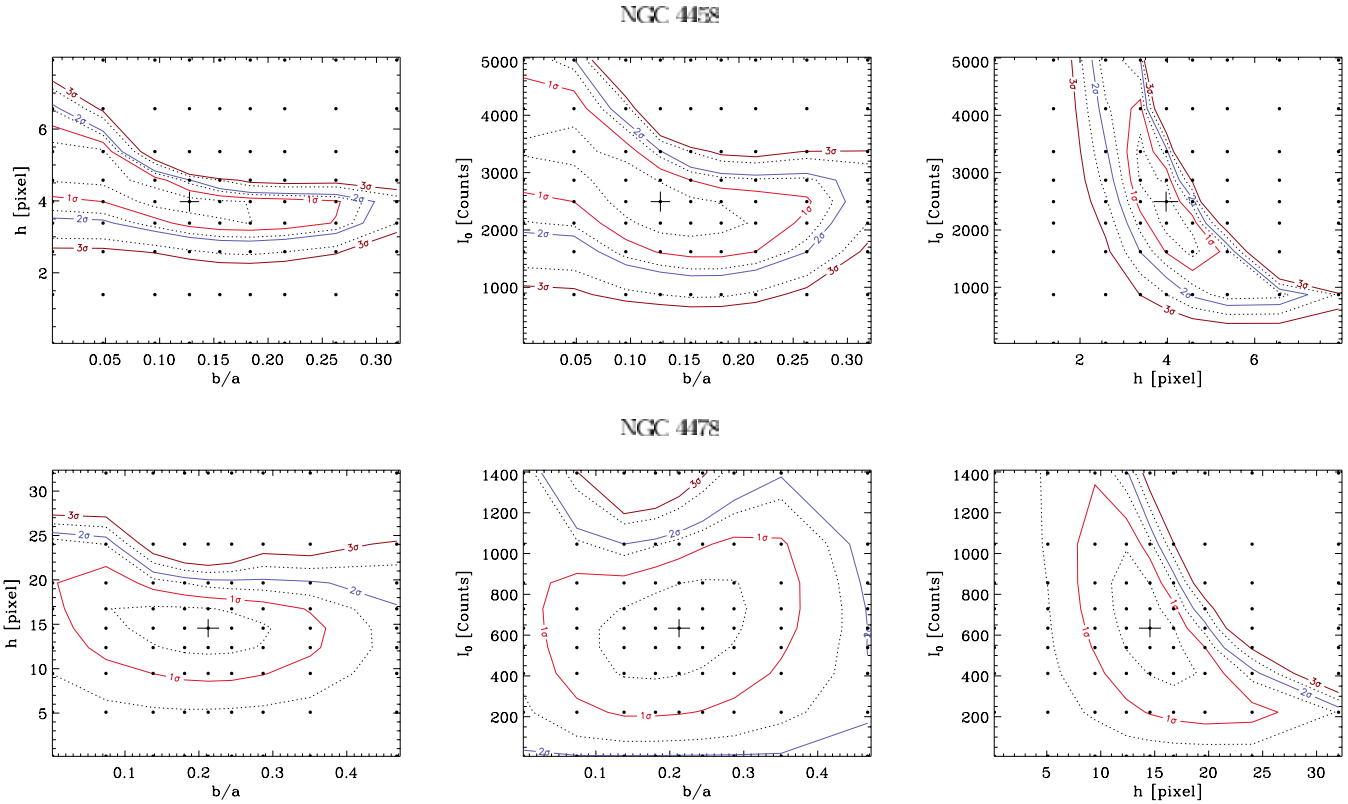

Figure 3. Contour plots of χ^2_ν for NGC 4458 (upper panels) and NGC 4478 (lower panels) as a function of the central surface brightness, I_0, scalelength, h, and axial ratio, b/a, of the nuclear disc models. Solid contours define the formal 68.3, 95.4 and 99.7 per cent confidence levels. Intermediate confidence levels are given by dashed contours. Filled circles indicate actual model calculations. Bi-cubic interpolation is used to calculate at χ^2_ν intermediate points. Crosses correspond to the best-fitting photometric parameters of the nuclear disc.

Table 1. Photometric parameters of the nuclear discs.

Name	$\mu_{0,V}$ (mag arcsec^{-2})	h (pc)	i (°)	$L_{\rm disc}$ ($L_{\odot,V}$)
NGC 4458	$14.74^{+0.71}_{-0.67}$	$11.0^{+5.9}_{-2.5}$	$83.1^{+6.9}_{-8.8}$	4.8×10^6
NGC 4478	$16.61^{+1.48}_{-0.81}$	$40.5^{+33.0}_{-18.7}$	$77.9^{+11.6}_{-10.0}$	1.9×10^7

$i = \arccos(b/a)$. The resulting values of central surface brightness in the V band, scalelength and inclination for both NSDs are listed in Table 1.

The disciness of NGC 4458 and 4478 disappears after the subtraction of the best-fitting model of the NSD as it results from the elliptical shape of their isophotes, as shown by the photometric profiles plotted in Fig. 2. We have tested that the result of the photometric decomposition is independent of position on the PC chip where the PSF is built. The resulting fraction of total luminosity contributed by the nuclear disc of NGC 4458 and 4478 is plotted as a function of radius in Fig. 2.

2.3.2 Photometric parameters of the nuclear discs with the Seifert & Scorza method

In applying the decomposition method by SB95, we assumed that the surface-brightness profile of the NSDs was exponential. To verify this assumption, we derived the surface-brightness profile of the NSDs using the alternative method of (Seifert & Scorza 1996, hereafter SS96). This decomposition method was developed to identify embedded discs in ellipticals and bulges without any a priori assumptions of the parametric law for their surface-brightness profile. In the deconvolved image of the galaxy, we masked the region of the NSD with a double-cone mask, and fit ellipses to the isophotes in the remaining part of image using the IRAF task ELLIPSE to derive the photometric properties of the host galaxy. A double-cone mask centred on the galaxy major axis is an optimal choice for the highly-inclined NSDs of NGC 4458 and 4478 because we expect that the isophotes close to the galaxy minor axis will be only slightly contaminated by light from the NSDs. The very central portion of the galaxy image was not masked to allow meaningful isophotes to be fitted. These masks correspond to the central 3×3 pixel (0.14×0.14 arcsec^2) of NGC 4458 and 5×5 pixel (0.23×0.23 arcsec^2) of NGC 4478. The opening angle of the mask ($\approx 90°$) was adjusted to minimize the influence of the NSD on the fitted parameters of the surrounding galaxy bulge component, but to ensure that a sufficient number of data points for the model derivation remained. A model was constructed to have perfectly elliptical isophotes with the same surface brightness, ellipticity and position angle radial profiles which we obtained from the isophotal fit. We subtracted the galaxy model from the original image to obtain a residual image which shows an elongated structure, namely the NSD, responsible for the higher-order deviations from perfectly elliptical isophotes. We extracted the surface-brightness radial profile along the major axis of the residual disc, which was close to being exponential. Scalelengths are consistent within their errors to those measured using the SB95 method, while the central surface brightnesses are somewhat fainter. This discrepancy in the surface brightnesses derived for using the SB95 and SS96 methods is a result of the actual shape of the double-cone mask where we excluded the central region in order to allow meaningful isophotes to be fitted. In this way, the observed central surface brightness is assigned to the host galaxy and the central surface brightness of the NSD is therefore underestimated.

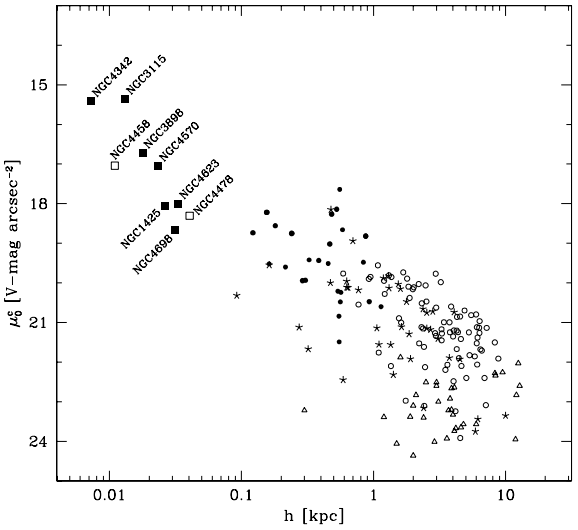

Figure 4. Disc $\mu_0^{\rm c}$–h diagram adapted from Pizzella et al. (2002). Open circles denote high surface-brightness spirals, triangles low surface-brightness spirals, stars S0s, and filled circles discy ellipticals. Large squares represent NSDs in elliptical galaxies (open symbols) and in S0s and spiral galaxies (filled symbols).

2.4 Structural parameters of nuclear discs

It is interesting to compare the scalelengths given in Table 1 ($h \approx 0.2$ arcsec for NGC 4458 and $h \approx 0.7$ arcsec for NGC 4478) with the 'break' radii found in the major and minor axes kinematics of the two galaxies (Halliday et al. 2001). Counter-rotation of about (30 km s^{-1}) is observed in the inner 4 arcsec of the major axis of NGC 4458. In the case of NGC 4478, the velocity dispersion drops in the central 2 arcsec, where the rotational velocity along the major axis drops by $\approx$20 km s^{-1} from 50 km s^{-1} at 2 arcsec to 30 km s^{-1} at 3 arcsec from the centre to increase again at larger radii.

Clearly, the spatial resolution of the kinematic data (see Section 3 for details) is smearing the signal of the NSDs. Fig. 4 shows the position of the NSDs of NGC 4458 and 4478 in the disc $\mu_0^{\rm c}$–h diagram (adapted from Pizzella et al. (2002); but see also van den Bosch 1998; Graham 2001). The face-on central surface brightness $\mu_0^{\rm c}$ has been derived from the observed one μ_0 by applying the following inclination correction

$$\mu_0^{\rm c} = \mu_0 - 2.5 \log(\cos i) \qquad (2)$$

and without taking into account any correction for extinction. The (small) scalelength and (high) central surface brightness of the disc of NGC 4458 are typical for NSDs. In contrast, the (relatively large) scalelength and (relatively low) central surface brightness of the disc of NGC 4478 are in between the typical values found for discy ellipticals and NSDs. No correlations are found with global properties (e.g. luminosity, scalelength, disc-to-bulge ratio) of the host galaxies.

Finally, on a speculative line of thought without presumption of rigourness, it is interesting to correlate the order of magnitude rotational velocities estimated above (30 km s^{-1} for NGC 4458 and 50 km s^{-1} for NGC 4478) with the estimated magnitudes of the discs. We find that discs following the Tully–Fisher relation (as in Haynes et al. 1999), and having the same rotational velocities, are expected to be $\approx$3 mag brighter than the NSDs of NGC 4458 and 4478. In other words, the NSDs of NGC 4458 and 4478 rotate faster than discs of the same luminosity that follow the Tully–Fisher relation. Taken at face value, this might indicate that they behave like test

particles embedded in the dominant gravitational potential generated by the main (bulge) body of the galaxies. However, the situation is complicated by the low spatial resolution of the kinematic data. Using the total masses of the discs derived in Section 4, we estimate that maximum rotational velocities of the order of ≈30–50 km s^{-1} are generated by the NSDs alone around 0.6–2 arcsec. Clearly, higher-resolution kinematic data and proper modelling (including a decomposition of the line-of-sight velocity distributions and seeing convolution) are needed to pin down the issue.

3 LINE-STRENGTH INDICES

Absorption line-strength indices are taken from a study of the stellar populations and kinematics of low-luminosity elliptical galaxies, in the Virgo cluster and nearby groups (Halliday 1999; Halliday et al. 2001). We provide a brief summary of our spectroscopic observations. Long-slit spectroscopic data were obtained using the Blue Channel Spectrograph at the Multiple Mirror Telescope, Arizona (USA). A Loral 3k × 1k CCD chip with a pixel size of 15 × 15 μm^2, a grating of 1200 slits mm^{-1} and a slit width of 1 arcsec were used. The spectral resolution was ∼1.5 Å FWHM, wavelength range 4555–6045 Å and spatial scale 0.6 arcsec $pixel^{-1}$. Seeing varied between 0.5 and 0.8 arcsec during observations. The reader is referred to Halliday (1999) for details of the spectroscopic data reduction and to Halliday et al. (2001) for a description of the kinematical analyses.

3.1 Measurement of absorption line-strength indices

Line-strength indices were measured as a function of radius to approximately one photometric effective radius along the major and minor axes of each galaxy. One-dimensional spectra were extracted for different luminosity-weighted radii of each axis and line-strength indices were measured for each spectrum using an algorithm developed by G. Baggley and revised by H. Kuntschner (Halliday 1999). The Lick/Image Dissector Scanner (IDS) system line-strength index definitions of Trager et al. (1998) were adopted. A fuller description of the algorithm is given below.

The principal input was a spectroscopic CCD frame for which basic data reduction had been completed. Before extracting one-dimensional spectra, the galaxy spectrum was checked to be aligned with the rows of the CCD frame. Using the IRAF tasks APFIND and APTRACE the position of the galaxy centre was traced along the dispersion axis; this step was performed to an accuracy of ≃0.03 pixels rms. The pixels were resampled such that the galaxy spectrum was centred on the same row pixel position as a function of dispersion.

One-dimensional spectra were extracted by summing rows of the galaxy frame until a signal-to-noise (S/N) ratio of 40 $Å^{-1}$ (for the wavelength range ∼5100–5300 Å) was attained. The dispersion axes of extracted spectra were rebinned to logarithmic intervals of wavelength. Redshifts were measured using the IRAF task FXCOR, by cross-correlating each spectrum with a range of one-dimensional de-redshifted stellar spectra. The mean redshift determined for all templates was used to de-redshift each galaxy spectrum. Hβ, Mg b, Fe5270 and Fe5335 line-strength indices were measured for all spectra. Errors for these raw index measurements were calculated based on Poissonian noise, the typical sky level counts subtracted during sky subtraction, and the values of readout noise and gain of the CCD.

Our line-strength index measurements were transformed to the Lick/IDS system. This procedure involved two steps: (i) correction to zero galaxy velocity dispersion; (ii) correction to the Lick/IDS spectral resolution (∼8.6 Å).

To correct for the effects of galaxy velocity dispersion, σ, different stellar spectra were smoothed by Gaussians corresponding to measurements of σ between 0 and 300 km s^{-1} in intervals of 20 km s^{-1}. Smoothing was performed using the IRAF task GAUSS. Correction factors for different values of σ were calculated for each index by comparing line index measurements for each smoothed spectrum with measurements for the original unsmoothed stellar spectrum. For the atomic indices Hβ, Mg b, Fe5270 and Fe5335, correction factors were defined to be the ratio of measurements for the original unbroadened stellar spectrum, $I_{\rm orig}$, and that for the spectrum broadened to a particular velocity dispersion, I_σ, i.e.

$$C(\sigma) = \frac{I_{\rm orig}}{I_\sigma}. \quad (3)$$

Mg b, Fe5270 and Fe5335 line-strength index measurements were corrected for the effects of σ using the calibrations for 12 stellar observations; for Hβ data, eight stellar observations were used. Linear relations were interpolated between the mean correction factor for each σ. The correction factor for an arbitrary measurement of σ was determined using the linear relation for the σ range bracketing the σ measurement. The measurement of σ as a function of radius was presented for both galaxies in Halliday et al. (2001). We adopt the σ measurements obtained for a S/N ≃ 60 $Å^{-1}$. Measurements of σ with S/N = 30 $Å^{-1}$ were adopted at large radii where uncertainties were larger.

Absorption line-strength index measurements and measurements of σ from Halliday et al. (2001) were measured in general for different galactic radii. Linear interpolations were made between neighbouring measurements of σ. A σ measurement for a radius at which line-strength indices were measured was found by linear interpolation from bracketing data. Depending on the appropriate side of the galaxy, if the radius was either less than or exceeded the radius of the most reliable measurement of σ, the linear interpolation determined for the closest radial interval was used to determine σ. The errors of line-strength index measurements corrected for galaxy velocity dispersion were calculated to be

$$\delta I_{\rm atomic}(\sigma) = \sqrt{[\delta I_{\rm orig} C(\sigma)]^2 + [I_{\rm orig}\delta C(\sigma)]^2}. \quad (4)$$

Here, $\delta I_{\rm orig}$ is the error in the raw measurement calculated as outlined above and $\delta C(\sigma)$ is the addition in quadrature of the standard deviations of correction factors for measurements of σ bracketing the σ measurement.

Corrections for the difference between our spectral resolution and the resolution of the Lick/IDS system were applied. A simulated Lick aperture was extracted for the major axis spectrum of each galaxy studied by Halliday (1999) present in the 'pristine' IDS sample of Trager (1997). Spectra were resampled such that the galaxy centre was aligned with the same pixel row position as a function of wavelength. For our spectroscopic slit width of 1 arcsec and spatial scale of 0.6 arcsec $pixel^{-1}$, a one-dimensional spectrum corresponding to a Lick/IDS aperture was created by summing the central nine rows (i.e. the central ∼5.4 arcsec of each galaxy spectrum). Line-strength indices were measured using the Lick/IDS definitions of Trager et al. (1998). The galaxy velocity dispersion was measured using the IRAF task FXCOR. Line-strength indices were corrected for the effects of σ using the calibrations discussed above. Direct comparisons were made with the fully-corrected Lick/IDS 1.4 × 4.0 $arcsec^2$ aperture measurements of the 'pristine' IDS sample of Trager (1997); we considered the Lick/IDS Hβ measurements corrected for the effects of σ but uncorrected for Hβ emission. Relation fitting was attempted between the simulated Lick/IDS aperture measurements corrected for σ and the Lick/IDS measurements of

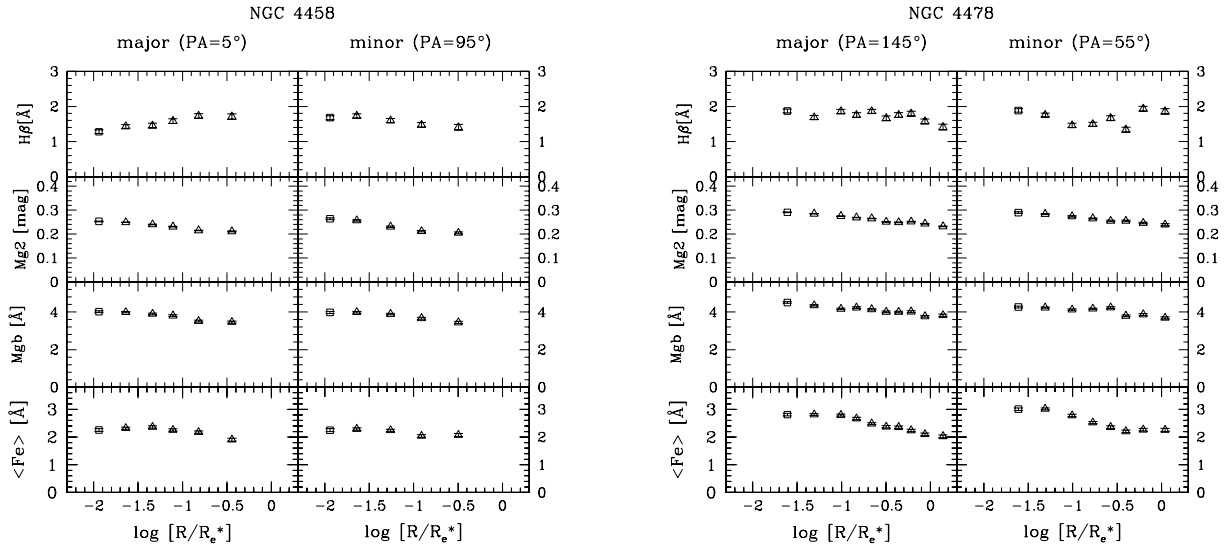

Figure 5. The radial profiles of the line-strength indices measured along the major and minor axes of NGC 4458 (left panels) and NGC 4478 (right panels). Squares refer to the value of line-strength indices measured at the galaxy centre.

Trager (1997), as a function of our σ-corrected, simulated Lick/IDS aperture measurements. After testing various routines, the median value of offset was found to provide a good fit for all line-strength indices (i.e. for Hβ, 0.272; Mg_2, -0.048; Mg_b, 0.051; Fe5270, 0.544; Fe5335, 0.697). The σ-corrected measurements were established on to the Lick/IDS system by subtracting these median values for all index measurements excluding Mg b, for which no zero correction was required because of the large scatter of offset values around the median.

3.2 Absorption line-strength gradients

Absorption line-strength index measurements for Hβ, Mg b, Mg_2 and $\langle Fe\rangle = (Fe5270 + Fe5335)/2$ are shown as a function of radius for the major and minor axes of NGC 4458 and 4478 in Fig. 5. Line-strength measurements are presented as a function of the normalized radius R/R_e^*, where $R_e^* = R_e/\sqrt{1-\epsilon}$ for the major axis and $R_e^* = R_e\sqrt{1-\epsilon}$ for the minor axis. R_e is the circularized effective radius defined as $R_e = A_e/2$ where A_e is the diameter of the circle enclosing one-half of the B-band total flux (RC3), and ϵ is the mean ellipticity of the galaxy. We assume $R_e = 26.1$ arcsec (RC3; corresponding to 1.6 kpc at the adopted distance) and $\epsilon = 0.00$ (Lauer et al. 1995) for NGC 4458, $R_e = 13.4$ arcsec (RC3; corresponding to 0.8 kpc at the adopted distance) and $\epsilon = 0.17$ (Peletier et al. 1990) for NGC 4478. The different central values measured along the major and minor axes for the same index give an estimate of the true measurement errors. Measurements for Mg_2 are shown for completeness and the calibration of this molecular index to the Lick/IDS system is described in Halliday (1999).

For NGC 4478, measurements of Hβ, Mg b, Mg_2, Fe5270, Fe5335 and $\langle Fe\rangle$ were derived previously for the galaxy centre by González (1993) and Trager et al. (1998), and as a function of radius of the major axis by Peletier (1989) and Gorgas, Efstathiou & Aragón-Salamanca (1990). In Fig. 6 we compare all previous measurements with our measurements presented here.

Good agreement within all margins of uncertainty is found between our data and the measurements of Peletier (1989). Measurements and errors for Fe5270 were not tabulated by Peletier (1989) and have been derived using the corresponding measurements of

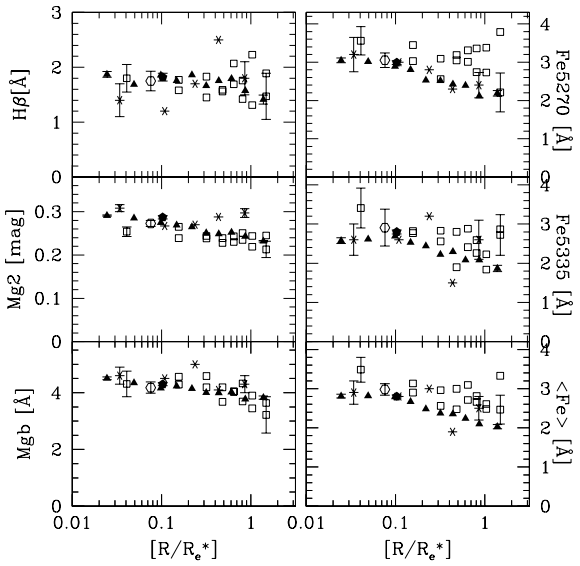

Figure 6. Comparison of our line-strength index data for NGC 4478 measured as a function of radius of the major axis (shown by filled triangles), the data Gorgas et al. (1990, open squares) and Peletier (1989, asterisks). The central measurements of González (1993, pentagon) and Trager et al. (1998, hexagon) are shown for representative radii. Error bars are provided for data at the innermost and outermost radii and the central measurements.

Fe5335 and $\langle Fe\rangle$. Agreement within the errors is found between our measurements and those of Gorgas et al. (1990) for Hβ and Mg b but not for Fe5270, Fe5335 and $\langle Fe\rangle$. A single bad pixel column was interpolated for a region corresponding to the red passband of Fe5270 of our spectrum of NGC 4478, but this is unlikely to be the cause of the discrepancy here because no evidence of unsuccessful bad pixel correction was found. Because Fe5270, Fe5335 and $\langle Fe\rangle$ are critical indices in the study of stellar populations, it has to be noted that our results are based on our data. At the galaxy centre, there is a small difference between our value of the Mg_2 index and that of Gorgas et al. (1990), while agreement within the errors is found for data at all other radii. The central measurements of the

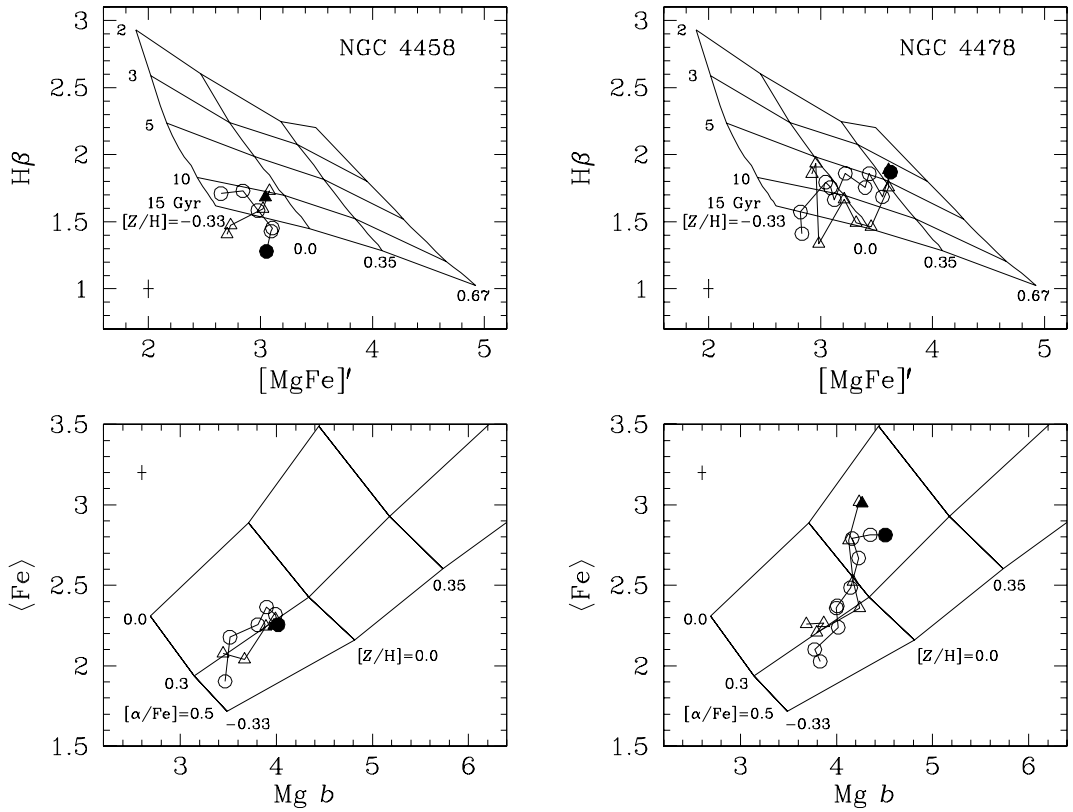

Figure 7. Top panels: the line strength of the Hβ and [MgFe]$'$ indices at different positions in the galaxies NGC 4458 (left panel) and NGC 4478 (right panel). The grid shows the models of Thomas et al. (2003) for different metallicities [Z/H] and ages. Bottom panels: the line strength of the Mg b and ⟨Fe⟩ indices at different positions in the galaxies NGC 4458 (left panel) and NGC 4478 (right panel). In all panels, the circles show the major axis, the triangles the minor axis, and the filled symbols the galaxy centres. The grid shows the models of Thomas et al. (2003) for different overabundances [α/Fe] and metallicities [Z/H], with an age of 12 Gyr.

line-strength indices of González (1993) and Trager et al. (1998) are in good agreement with our measurements.

4 AGES, METALLICITIES AND α/Fe OVERABUNDANCES

In the following we indicate the combined magnesium–iron index with

$$[\mathrm{MgFe}]' = \sqrt{\mathrm{Mg}\,b(0.72 \times \mathrm{Fe5270} + 0.28 \times \mathrm{Fe5335})} \qquad (5)$$

newly defined by TMB. This index is completely independent of the [α/Fe] overabundance and hence serves best as a metallicity tracer.

We show in the top panels of Fig. 7 the line strengths of the Hβ and [MgFe]$'$ indices at different positions in the galaxies NGC 4458 and 4478 with the grid of models of TMB. No clear trend is observed for NGC 4458. NGC 4478 shows a negative gradient in both the indices Hβ and [MgFe]$'$. We show in the bottom panels of Fig. 7 the line strength of the Mg b and ⟨Fe⟩ indices at different positions in the galaxies NGC 4458 and 4478. For both galaxies, both indices ⟨Fe⟩ and Mg b decrease outward on the mean.

Using stellar population models with variable element abundance ratios from TMB, we derive average ages, metallicities and [α/Fe] ratios as a function of the position in the galaxies, following the procedure of Mehlert et al. (2003). Fig. 8 translates the trends observed in Fig. 7 as follows. NGC 4458 is uniformly old ($t \approx 15$ Gyr), has overall low metal content ([Z/H] ≈ -0.2) and overabundance ([α/Fe] ≈ 0.3). For NGC 4478 instead the central regions ($R < 0.1 R_e$) are younger ($t \approx 6$ Gyr), more metal rich ([Z/H] ≈ 0.35) and less overabundant ([α/Fe] ≈ 0.2) than the outer regions, where old ages ($t \approx 15$ Gyr), low metallicities ([Z/H] ≈ 0.1) and high overabundances ([α/Fe] ≈ 0.3) are observed on both the minor and the major axes. The size of the error bars shows that the decreases in age and overabundance in the central region are significant. Finally, note that, within the errors, most of the ages shown in Fig. 8 are compatible with the age of the Universe favoured by the *Wilkinson Microwave Anisotropy Probe* (Spergel et al. 2003). In the following we will interpret the radial variations described above as the result of the superposition of the central discs detected photometrically in Section 2.2 and the main body of the galaxy. Moreover, we will assume that the main body of the galaxy does not have a [α/Fe] gradient, in agreement with the results of Mehlert et al. (2003). NGC 4458 has properties similar to giant ellipticals with decoupled cores. Prototypes of decoupled cores in giant ellipticals are as old as, and more metal rich than, the rest of the galaxy, with high and approximately constant overabundance, as in the case of NGC 4816 and IC 4051 (Mehlert et al. 1998), or NGC 4365 (Surma & Bender 1995; Davies et al. 2001). In NGC 4458, the inner disc and the main body of the galaxy appear to have the same stellar populations, with a metallicity gradient for the main body of the galaxy slightly weaker than the cases discussed above. By contrast, the case of NGC 4478 is intriguing. The inner, cold disc is younger, richer in metals and less overabundant than the main body of the galaxy. We tested this conclusion with a composite stellar population model, summing 10 per cent of a young ($t = 1.65$ Gyr) and metal-rich

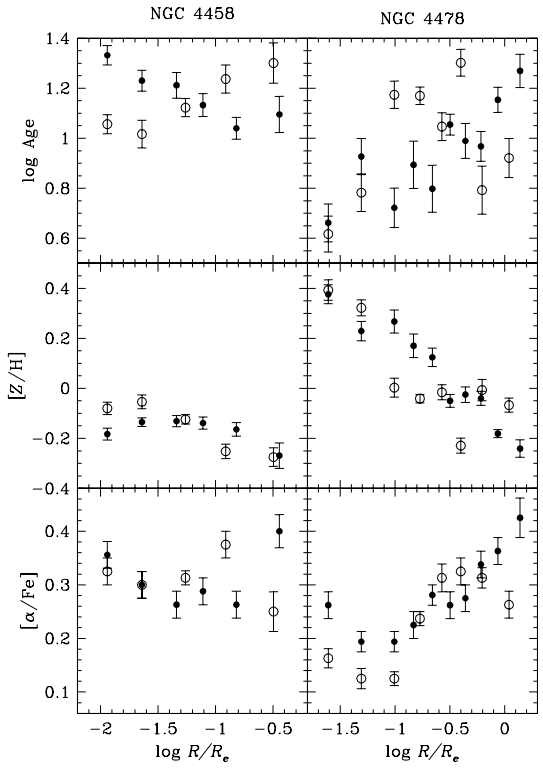

Figure 8. The age (top panels), metallicity [Z/H] (middle panels) and overabundance [α/Fe] (bottom panels) profiles as a function of the distance from the centre in units of half-luminosity radius derived from the Hβ, $\langle$Fe$\rangle$ and Mg b values using the models of Thomas et al. (2003). The filled symbols refer to the major axis of the galaxies, and the open symbols to the minor axis.

($Z = 3\ Z_\odot$) component with solar α/Fe ratios, and 90 per cent of an old ($t = 12$ Gyr) metal-rich ($Z = 2\ Z_\odot$) overabundant ([α/Fe] = 0.4) population, and recovering the observed central values of the line indices. Given the errors of the available spectroscopic data and their spatial resolution, we refrained from a detailed study of the allowed range of alternative solutions, which only spectroscopy at *HST* resolution can pin down.

Of course, higher than solar α/Fe ratios for the disc are allowed if we relax the assumption that the α/Fe ratio of the main body of NGC 4478 is constant. Using these age and metallicity estimates and the models of Maraston (1998), we compute that the mass-to-light ratios of the inner discs are $M/L_V = 7.2\ M_\odot/L_\odot$ for NGC 4458 (with a range from 5 to 10 judged from the range of ages and metallicities shown in Fig. 8) and $M/L_V = 1.3\ M_\odot/L_\odot$ for NGC 4478. In this case, given the limitations of the spectroscopic data discussed above, the uncertainties are probably as large as a factor of 2. Combined with the luminosities given in Table 1, this gives masses of $M = 3.4 \times 10^7\ M_\odot$ and $M = 2.5 \times 10^7\ M_\odot$, respectively. The kinematic and photometric properties discussed above argue for the presence of (cold) discs at the centres of NGC 4458 and 4478, and therefore for a formation scenario through the dissipational collapse of a gas-rich object. The observed kinematic signature of counter-rotation in NGC 4458 argues in addition for an external origin with decoupled angular momentum. The absence of gradients in the stellar population of NGC 4458 indicates that the formation of the inner cold structure occurred at the same time as the main body of the galaxy. The younger age and low overabundance of the central structure of NGC 4478 is indicative of a prolonged star formation history (Thomas, Greggio & Bender 1999), typical of an undisturbed disc-like, gas-rich (possibly pre-enriched) structure. This is consistent with the absence of counter-rotation.

5 CONCLUSIONS

We have investigated the properties of the central regions of the low-luminosity ellipticals NGC 4458 and 4478, finding the following.

(i) *HST* archive images of the two galaxies show the presence of central discs. They have scalelengths and face-on central surface brightnesses which fit on the μ_0^c–h relation for galaxy discs. For NGC 4458, these parameters are typical of NSDs, while for NGC 4478 they are intermediate between the values for NSDs and the discs of discy ellipticals.

(ii) Measurements presented by Halliday et al. (2001) along the major and minor axes of the galaxies revealed the presence of decoupled kinematics on the radial scales of the NSDs. A counter-rotating central structure is present in NGC 4458, a cold rotating component in NGC 4478.

(iii) The Lick/IDS absorption line-strength indices Hβ, Mg b and $\langle$Fe$\rangle$, measured as a function of radius along the major and the minor axes of the galaxies, allow us to estimate the age, metallicity and overabundance of the stellar populations of the two galaxies using simple stellar population models.

(iv) The radial variations of the derived quantities constrain the stellar population properties of the central discs. The NSD of NGC 4458 has an estimated stellar mass of $3.4 \times 10^7\ M_\odot$ and is similar to the decoupled cores of bright ellipticals, being as old as and richer in metals than the rest of the galaxy, with high and approximately constant overabundance. The cold central disc of NGC 4478 has a similar estimated stellar mass of $2.5 \times 10^7\ M_\odot$, but is younger, richer in metals and less overabundant than the main body of the galaxy.

(v) The nearly solar α-element abundance of the central disc of NGC 4478 indicates a prolonged star formation history, typical of an undisturbed disc-like, gas-rich (possibly pre-enriched) structure.

ACKNOWLEDGMENTS

This work is based on observations made with the NASA/ESA *HST*, obtained from the data archive at the STScI. STScI is operated by the AURA, Inc., under the NASA contract NAS 5-26555. We thank the observing committee of the Harvard–Smithsonian Center for Astrophysics (CfA) for their generous award of telescope time to obtain the spectroscopic observations presented here. The spectroscopic absorption line-strength measurements presented were derived as part of the PhD thesis research of CH. CH gratefully acknowledges the support of a UK Particle Physics and Astronomy Research Council (PPARC) studentship at the University of Durham, the grant support of the Italian National Research Centre (grant CNRG00887) and a grant from the Fondo per gli Investimenti della Ricerca di Base of the Italian Ministry of Education, University and Research (grant RBAU018Y7E). We acknowledge A. W. Graham for useful discussion. LM gratefully acknowledges the support of a European Southern Observatory (ESO) studentship at the ESO Research Facilities in Santiago. RPS is grateful for the financial support by the DFG grant SFB375. This research has made use of the Lyon–Meudon Extragalactic Data base (LEDA), the NASA/IPAC Extragalactic Database (NED) and Starlink facilities.

REFERENCES

Arnold R., de Zeeuw P. T., Hunter C., 1994, MNRAS, 271, 984

Balcells M., Graham A. W., Domínguez-Palmero L., Peletier R. F., 2003, ApJ, 582, L79

Balcells M., Graham A. W., Peletier R. F., 2004, ApJ, submitted (astro-ph/0404381)

Bertola F., Corsini E. M., 1999, in Proc. IAU Symp. 186, Galaxy Interactions at Low and High Redshift. Kluwer, Dordrecht, p. 149

Bertola F., Corsini E. M., Vega Beltrán J. C., Pizzella A., Sarzi M., Cappellari M., Funes J. G., 1999, ApJ, 519, L127

Böker T., Laine S., van der Marel R. P., Sarzi M., Rix H., Ho L. C., Shields J. C., 2002, AJ, 123, 1389

Bruzual G., Charlot S., 2003, MNRAS, 344, 1000

Caon N., Capaccioli M., Rampazzo R., 1990, A&AS, 86, 429

Cappellari M., 2002, MNRAS, 333, 400

Carollo C. M., Danziger I. J., Rich R. M., Chen X., 1997, ApJ, 491, 545

Davies R. L., Sadler E. M., Peletier R. F., 1993, MNRAS, 262, 650

Davies R. L. et al., 2001, ApJ, 548, L33

de Vaucouleurs G., de Vaucouleurs A., Corwin J. R., Buta R. J., Paturel G., Fouque P., 1991, Third Reference Catalogue of Bright Galaxies (RC3)

Faber S. M., Friel E. D., Burstein D., Gaskell C. M., 1985, ApJS, 57, 711

Faber S. M. et al., AJ, 114, 1771

Ferrarese L., van den Bosch F. C., Ford H. C., Jaffe W., O'Connell R. W., 1994, AJ, 108, 1598

González J. J., 1993, Line Strength Gradients and Kinematic Profiles in Elliptical Galaxies, PhD thesis, Univ. California

Gorgas J., Efstathiou G., Aragón-Salamanca A. A., 1990, MNRAS, 245, 217

Graham A. W., 2001, MNRAS, 326, 543

Graham A. W., Guzmán R., 2003, AJ, 125, 2936

Halliday C., 1999, Low-Luminosity Elliptical Galaxies, PhD thesis, Univ. Durham

Halliday C., Davies R. L., Kuntschner H., Bender R., Birkinshaw M., Saglia R. P., Baggley G., 2001, MNRAS, 326, 473

Haynes M. P., Giovanelli R., Chamaraux P., da Costa L. N., Freudling W., Salzer J. J., Wegner G., 1999, AJ, 117, 2039

Holley-Bockelmann K., Richstone D. O., 2000, ApJ, 531, 232

Holtzman J. A. et al., 1995a, PASP, 107, 156

Holtzman J. A., Burrows C. J., Casertano S., Hester J. J., Trauger J. T., Watson A. M., Worthey G., 1995b, PASP, 107, 1065

Jaffe W., Ford H. C., O'Connell R. W., van den Bosch F. C., Ferrarese L., 1994, AJ, 108, 1567J

Jedrzejewski R., 1987, MNRAS, 226, 747J

Kinney A. L., Calzetti D., Bohlin R. C., McQuade K., Storchi-Bergmann T., Schmitt H. R., 1996, ApJ, 467, 38

Kobayashi C., Arimoto N., 1999, ApJ, 527, 573

Kormendy J., 1984, ApJ, 287, 577

Kormendy J., Bender R., 1996, ApJ, 464, L119

Kormendy J., Gebhardt K., 2001, in AIP Conf. Proc. 586, 20th Texas Symposium on Relativistic Astrophysics. American Institute of Physics, New York, p. 363

Kormendy J. et al., 1996, in Proc. IAU Symp. 171, New Light on Galaxy Evolution. Kluwer, Dordrecht, p. 105

Krist J., Hook R., 1999, STIS Instrument Handbook Version 4.0. STScI, Baltimore

Lauer T. R. et al., 1995, AJ, 110, 2622

Maraston C., 1998, MNRAS, 300, 872

Mehlert D., Saglia R. P., Bender R., Wegner G., 1998, A&A, 332, 33

Mehlert D., Saglia R. P., Bender R., Wegner G., 2000, A&AS, 141, 449

Mehlert D., Thomas D., Saglia R. P., Bender R., Wegner G., 2003, A&A, 407, 423

Michard R., 1985, A&AS, 59, 205

Monnet G., Bacon R., Emsellem E., 1992, A&A, 253, 366

Peletier R. F., 1989, PhD thesis, Univ. Groningen

Peletier R. F., Davies R. L., Illingworth G. D., Davis L. E., Cawson M., 1990, AJ, 100, 1091

Pizzella A., Corsini E. M., Morelli L., Sarzi M., Scarlata C., Stiavelli M., Bertola F., 2002, ApJ, 573, 131

Press W. H., Teukolsky S. A., Vetterling W. T., Flannery B. P., 1992, Numerical Recipes in FORTRAN. The Art of Scientific Computing. Cambridge Univ. Press, Cambridge

Prugniel P., Nieto J.-L., Simien F., 1987, A&A, 173, 49

Ravindranath S., Ho L. C., Peng C. Y., Filippenko A. V., Sargent W. L. W., 2001, AJ, 122, 653

Rest A., van den Bosch F. C., Jaffe W., Tran H., Tsvetanov Z., Ford H. C., Davies J., Schafer J., 2001, AJ, 121, 2431

Rix H. W., White S. D. M., 1992, MNRAS, 254, 389

Sandage A., Tammann G. A., 1981, Revised Shapley–Ames Catalogue of Bright Galaxies. Carnegie Institution, Washington (RSA)

Scorza C., Bender R., 1995, A&A, 293, 20 (SB95)

Scorza C., van den Bosch F. C., 1998, MNRAS, 300, 469

Seifert W., Scorza C., 1996, A&A, 310, 75 (SS96)

Spergel D. N. et al., 2003, ApJS, 148, 175

Surma P., Bender R., 1995, A&A, 298, 405

Tantalo R., Chiosi C., Bressan A., 1998, A&A, 333, 419

Thomas D., Greggio L., Bender R., 1999, MNRAS, 302, 537

Thomas D., Maraston C., Bender R., 2003, MNRAS, 339, 897 (TMB)

Tomita A., Aoki K., Watanabe M., Takata T., Ichikawa S., 2000, AJ, 120, 123

Trager S. C., 1997, The Stellar Population Histories of Elliptical Galaxies, PhD thesis, Univ. California

Trager S. C., Worthey G., Faber S. M., Burstein D., González J. J., 1998, ApJS, 116, 1

Tran H. D., Tsvetanov Z., Ford H. C., Davies J., Jaffe W., van den Bosch F. C., Rest A., 2001, AJ, 121, 2928

Trujillo I., Erwin P., Ramos A. A., Graham A. W., 2004, AJ, 127, 1917

Tully R. B., 1988, Nearby Galaxy Catalogue. Cambridge Univ. Press, Cambridge

van den Bosch F. C., 1998, ApJ, 507, 601

van den Bosch F. C., Emsellem E., 1998, MNRAS, 298, 267

van den Bosch F. C., Ferrarese L., Jaffe W., Ford H. C., O'Connell R. W., 1994, AJ, 108, 1579

van den Bosch F. C., Jaffe W., van der Marel R. P., 1998, MNRAS, 293, 343

van Dokkum P. G., Franx M., 1995, AJ, 110, 2027

Vazdekis A., 1999, ApJ, 513, 224

Worthey G., 1994, ApJS, 95, 107

This paper has been typeset from a TEX/LATEX file prepared by the author.